

Article

Simulating and Comparing CO₂/CH₄ Separation Performance of Membrane–Zeolite Contactors by Cascade Neural Networks

Seyyed Amirreza Abdollahi ¹, AmirReza Andarkhor ², Afham Pourahmad ³, Ali Hosin Alibak ^{4,5},
Falah Alobaid ⁶ and Babak Aghel ^{6,7,*}

¹ Faculty of Mechanical Engineering, University of Tabriz, Tabriz 5166616471, Iran

² Department of Chemistry, Payam Noor University (Bushehr Branch), Bushehr 1688, Iran

³ Department of Polymer Engineering, Amirkabir University of Technology, Tehran 1591634311, Iran

⁴ Chemical Engineering Department, Faculty of Engineering, Soran University, Soran 44008, Iraq

⁵ Faculty of Chemical and Petroleum Engineering, University of Tabriz, Tabriz 5166616471, Iran

⁶ Institut Energiesysteme und Energietechnik, Technische Universität Darmstadt, Otto-Berndt-Straße 2, 64287 Darmstadt, Germany

⁷ Department of Chemical Engineering, Faculty of Energy, Kermanshah University of Technology, Kermanshah 6715685420, Iran

* Correspondence: babak.aghel@est.tu-darmstadt.de; Tel.: +49-6151-16-22673; Fax: +49-(0)-6151-16-22690

Abstract: Separating carbon dioxide (CO₂) from gaseous streams released into the atmosphere is becoming critical due to its greenhouse effect. Membrane technology is one of the promising technologies for CO₂ capture. SAPO-34 filler was incorporated in polymeric media to synthesize mixed matrix membrane (MMM) and enhance the CO₂ separation performance of this process. Despite relatively extensive experimental studies, there are limited studies that cover the modeling aspects of CO₂ capture by MMMs. This research applies a special type of machine learning modeling scenario, namely, cascade neural networks (CNN), to simulate as well as compare the CO₂/CH₄ selectivity of a wide range of MMMs containing SAPO-34 zeolite. A combination of trial-and-error analysis and statistical accuracy monitoring has been applied to fine-tune the CNN topology. It was found that the CNN with a 4-11-1 topology has the highest accuracy for the modeling of the considered task. The designed CNN model is able to precisely predict the CO₂/CH₄ selectivity of seven different MMMs in a broad range of filler concentrations, pressures, and temperatures. The model predicts 118 actual measurements of CO₂/CH₄ selectivity with an outstanding accuracy (i.e., AARD = 2.92%, MSE = 1.55, R = 0.9964).

Keywords: CO₂/CH₄ gas mixture; membrane separation; selectivity; intelligent modeling



Citation: Abdollahi, S.A.; Andarkhor, A.; Pourahmad, A.; Alibak, A.H.; Alobaid, F.; Aghel, B. Simulating and Comparing CO₂/CH₄ Separation Performance of Membrane–Zeolite Contactors by Cascade Neural Networks. *Membranes* **2023**, *13*, 526. <https://doi.org/10.3390/membranes13050526>

Academic Editors: Eric Favre and Ivo F.J. Vankelecom

Received: 27 March 2023

Revised: 2 May 2023

Accepted: 17 May 2023

Published: 18 May 2023



Copyright: © 2023 by the authors. Licensee MDPI, Basel, Switzerland. This article is an open access article distributed under the terms and conditions of the Creative Commons Attribution (CC BY) license (<https://creativecommons.org/licenses/by/4.0/>).

1. Introduction

Developing carbon capture and sequestration technologies, deploying renewable sources of energy, and tightening the regulations are the key strategies to achieve the Paris Agreement targets [1,2]. To this end, among different renewable energies such as solar, wind, biogas, and biomass, biogas has already demonstrated an appealing potential to be replaced with fossil fuels [3]. On the other hand, to meet the pipeline safety and maintenance criteria, biogas requires upgrading by separating the bio-methane from the involved contaminants, such as carbon dioxide [4]. Accordingly, separating the CO₂/CH₄ is not only necessary for climate change mitigation, but also favorable for synthesizing the value-added chemicals [5]. To date, several different technologies including electrochemical reduction [6], membrane [7], cryogenic [8], adsorption [9], and absorption [10] have been investigated for gas capture and sequestration. Selectivity is one of the key factors of the membrane-based separation processes [11].

Among these strategies, absorption and cryogenic ones are the most mature, while absorption represents some serious environmental problems and cryogenics consume a

high amount of energy [12,13]. In addition, membrane technology which is efficient and environmentally friendly appears as the most interesting for gas capture and separation [14]. On these grounds, in recent decades, numerous studies have been devoted to developing different types of membranes or improving their performance [14]. Some of the recent interesting ones can be found in [14,15].

Routinely, polymeric membranes are known for their high modular specific area, and ease of processing [16,17], while the low separation performance because of the Robeson upper bound is the major drawback of these types of membranes [18,19]. Furthermore, low permeability and selectivity are the other limitations of polymeric membranes for large-scale sequestration [20]. To cover these impediments, mixed matrix membranes (MMMs) emerged to improve the polymer's separation performances by incorporating the textural characters of carbon molecular sieves or zeolites in the conventional polymer matrixes [19]. It is worth mentioning that adding the inorganic fillers to the polymeric matrix and developing highly efficient membranes involves some hardness, including weak contact and/or poor distribution of the fillers in the considered polymer matrix [14,19]. Furthermore, fabricating MMMs is influenced by the loading of filler, particle size, polymer properties, and also filler pore size [14,21].

Accordingly, zeolites based on their particular characteristics, i.e., crystallinity, uniformity, and ion exchange potential, have provided an excellent capacity for different areas of gas capture and sequestration [22,23]. Among various introduced zeolites, SAPO-34 zeolite is considered a unique one concerning its interesting specifications including pore diameter, medium acidity, selectivity, high stability, and kinetic diameter for separating CH₄ and CO₂ in related applications such as biogas upgrading and natural gas sweetening [24,25]. Many researchers experimentally investigated the CO₂/CH₄ selectivity of the MMMs containing SAPO-34 as a function of pressure, temperature, filler dosage, and polymer type (see the next section). The review article written by Rimaz et al. presents several interesting illustrations of the SAPO-34 zeolite which help readers understand the chemistry of this zeolite [26]. Routinely, selectivity experimental measurement is costly, time-consuming, and is affected by human-caused errors.

On the other hand, machine learning (ML) approaches have received significant interest for the intelligent simulating of a wide range of problems [27–29]. To this end, fault detection [30], pattern recognition [31], data mining [32], and model deriving [33] are some of the main covered domains by ML. Lately, several different ML topologies, including artificial neural networks (ANN) [34], support vector machines [35], adaptive neuro-fuzzy inference systems (ANFIS) [36], and genetic programming [37] have been employed in membrane technology. In this way, Zhao et al. evaluated membrane-fouling criteria in a membrane bioreactor for the estimation of interfacial interactions using ANN [38]. They reported the robust potential of the radial basis function for the prediction of interfacial interactions. Additionally, Tyagi et al. coupled artificial neural networks with genetic algorithms to optimize and model neodymium ion separation by a liquid membrane [39]. Furthermore, Rezakazemi et al. employed different ML approaches including ANFIS, PSO, and GA to estimate the selectivity of hydrogen in mixed matrix membranes [36]. Additionally, the maps for process evaluation for membrane-based CO₂ separation technology were also developed by Gasós et al. using artificial neural networks [40].

In the current study, a robust intelligent model has been proposed to estimate the selectivity of mixed matrix membranes containing SAPO-34 zeolite for the separation of CO₂ and CH₄. The suggested model is novel, precise, and could anticipate the effect of different variables on the carbon dioxide and methane separation performance of MMMs. The proposed model also provides a grounding for synthesizing an MMM with the maximum carbon dioxide and methane separation efficiency.

2. Materials and Methods

2.1. Data Collection

As already discussed, SAPO-34 zeolite is one of the favorable zeolites in fabricated MMMs, which has been extensively investigated in the literature by several research groups [41–52]. On these grounds, an extensive experimental database of MMMs with different percentages of SAPO-34 zeolite was gathered from the literature [41–52] to ensemble a CNN-based paradigm for estimating the CO₂/CH₄ selectivity at different pressures and temperatures. Several substrates, including polyurethane, polysulfone, polytherysulfone, polyetherimide, Pebax 1657, Pebax 1074, and Matrimid 5218 have been checked in the literature [41–52]. As Table 1 shows, the database covers the filler dosage of 0–50 wt%, a temperature range of 298–348 K, and a pressure range of 0.1–3.0 MPa. In these ranges of experiments, the CO₂/CH₄ selectivity of MMMs varies from 1.38–66.99.

Table 1. Summary of the reported CO₂/CH₄ selectivity of MMMs in the literature [41–52].

Variable	Observations	Minimum	Maximum	Mean	St. Deviation
Filler dosage (wt%)	118	0	50	12.11	11.11
Temperature (K)	118	298	348	305.03	10.51
Pressure (MPa)	118	0.10	3.0	0.93	0.67
CO ₂ /CH ₄ selectivity	118	1.38	66.99	26.69	14.62

It must be mentioned that, although it is possible to simulate the effect of all influential variables on the CO₂/CH₄ selectivity using the CNN model, the following matters convinced us to only consider the effect of SAPO-34 dose, polymer type, temperature, and pressure on the selectivity.

1. The model is better to develop based on its easy and always available variables
2. Some of the potentially influential variables, including the MMM synthesis method and selectivity measurement procedure, are not reported in some of the original articles. Therefore, we have not considered them as independent variables.
3. It is better to ignore those variables that have a minor impact on the selectivity.

2.2. Dependency of CO₂/CH₄ Selectivity on Involved Variables

The previous section clearly defined both dependent and independent variables involved in methane and carbon dioxide separation by polymer/SAPO-34 membranes. Presently, Pearson's method is applied to reveal the relationship between each pair of dependent and independent variables. This method uses Equation (1) to identify the most possible pattern between a pair of variables (i.e., x and y) and extract their relationship [53].

$$PC_{x,y} = \frac{\sum_{k=1}^m (x_k - \bar{x})(y_k - \bar{y})}{\left(\sqrt{\sum_{k=1}^m (x_k - \bar{x})^2} \sqrt{\sum_{k=1}^m (y_k - \bar{y})^2} \right)} \quad (1)$$

Here $PC_{x,y}$ shows the Pearson's coefficients between independent (x) and dependent (y) variables. In addition, m stands for the number of available records, and k is an index determining the upper and lower bounds of the summation operator. The relationship type/strength is coded using a coefficient that varies between -1 and $+1$ [54]. The minimum and maximum coefficients show the strongest indirect and direct relationships, respectively. The physical meaning of other coefficients can also be inferred by their closeness to either the maximum or minimum bounds.

Figure 1 presents the Pearson's coefficients for the relationship of CO₂/CH₄ selectivity to the SAPO-34 dosage in MMMs, polymer type, temperature, and pressure. The selectivity directly relates to the first two independent variables, while it indirectly relates to the two

last variables. In addition, the selectivity dependency of the SAPO-34 dosage in MMMs and pressure are the strongest direct and indirect relationships, respectively.

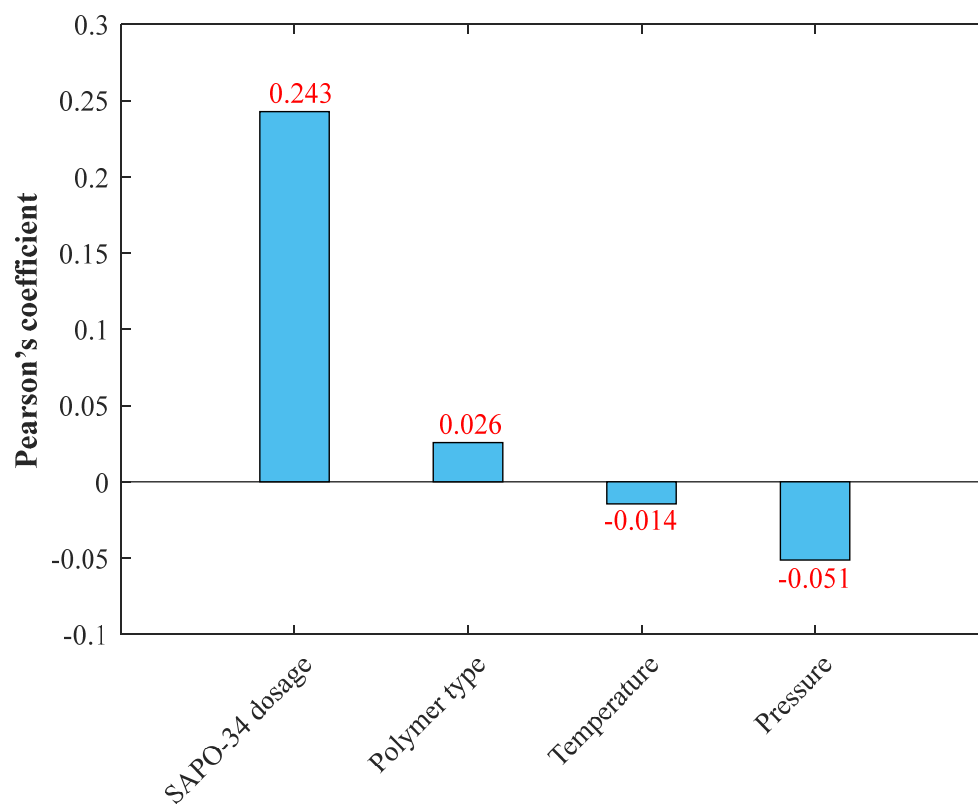


Figure 1. Pearson's coefficients for the dependency of CO_2/CH_4 selectivity of MMMs to the involved features.

It is better to note that the level of data scattering is a critical factor that often misleads the relevancy tests to provide inaccurate results. The literature clearly states that the Pearson's predictions are sometimes the opposite of those approved by scientific facts [53]. Although Pearson's method claimed that selectivity has almost no relationship with pressure and temperature, all experts in the field of membrane-based separation know that these are important variables and have a substantial impact on the operation.

It should also be mentioned that, since the polymer type is a qualitative variable, numerical indicators are applied to quantitatively present it. Indeed, polyurethane, polysulfone, polytherysulfone, polyetherimide, Pebax 1657, Pebax 1074, and Matrimid 5218 are coded by 1, 2, . . . , and 7, respectively.

2.3. Cascade Neural Networks (CNN)

ANN is a non-linear topology that was first developed according to the pattern of human brain processing for data analysis [55]. Accordingly, the flexibility, robustness, and accuracy of this strategy quickly nominated it in a broad range of applications from biomedicine to sustainable development [56,57]. It is possible to design a powerful ANN model to extract a logical pattern among the considered determinative factors, with related dependent ones, despite any degree of complexity [58]. To this end, providing an acceptable experimental dataset is a primary step in developing a black box for the prediction of targets [59]. In this way, the architecture of ANNs is obtained with signal analysis among the input and output factors. It is worth noting that the successful development of the ANN approach demands order specifications in different layers related to neuron interactions. Accordingly, various types of ANN topologies have been introduced such as multi-layer perceptron, cascade, radial basis function, and general regression [55]. Among these

paradigms, the cascade neural network (CNN) is considered the most popular tool to simulate different phenomena [60,61]. The CNN approach directly connects the input layer to all the next hidden/output layers [60]. Accordingly, in the current study, the CNN topology has been employed which includes three key layers such as input, hidden, and output. Here, the input layer is associated with independent factors (variables) that have already affirmed the most significant traces of the process, which, after some data analyses, are sent to the hidden layer. In this layer, the major data processing and mathematical treatment are applied; thereafter, the outcomes are introduced to the output layer for final analysis. The applied mathematical processing related to neurons is specified by Equation (2) as follows [62]:

$$NON = \sum_{r=1}^M w_r x_r + b \tag{2}$$

This equation states that the net output of a neuron (*NON*) can be calculated from the entry signal (i.e., $[x_1, x_1, \dots, x_M]^T$), weight vector (w_r), and a bias (b). Additionally, a transfer function (f) is supplied to receive the *NON* and calculate the outlet signal, i.e., $f(NON)$. Although there are various types of transfer functions [57], the current study uses the hyperbolic tangent sigmoid (Equation (3)) and logarithmic sigmoid (Equation (4)) in hidden and output layers, respectively [63].

$$f(NON) = \frac{\exp(NON) - \exp(-NON)}{\exp(NON) + \exp(-NON)} \tag{3}$$

$$f(NON) = \frac{1}{1 + \exp(-NON)} \tag{4}$$

It should be mentioned that to properly benefit from the normalization process to enhance the training rate as well as improve its quality, the logarithm sigmoid has been incorporated into the output layer. Indeed, all variables in our study have been normalized [0 1] before starting the model development phase.

2.4. Accuracy Measurement

This study relies on several accuracy criteria to measure the deviation between actual and predicted carbon dioxide to methane selectivity (*CMS*) of MMMs. The correlation of determination (*R*), absolute average relative deviation percent (*AARD%*), mean squared errors (*MSE*), relative deviation percent (*RD%*), and residual error (*RE*) are defined by Equations (5)–(9) and are used in the current study [64]:

$$R = \sqrt{1 - \left\{ \frac{\sum_{k=1}^m (CMS^{act} - CMS^{pred})_k^2}{\sum_{k=1}^m (CMS^{act} - \overline{CMS^{act}})_k^2} \right\}} \tag{5}$$

$$AARD\% = (100/m) \times \sum_{k=1}^m \left(\left| CMS^{act} - CMS^{pred} \right| / CMS^{act} \right)_k \tag{6}$$

$$MSE = (1/m) \times \sum_{k=1}^m \left(CMS^{act} - CMS^{pred} \right)_k^2 \tag{7}$$

$$RD\% = 100 \times \left(CMS^{act} - CMS^{pred} \right) / CMS^{act} \tag{8}$$

$$RE = \left(CMS^{act} - CMS^{pred} \right) \tag{9}$$

where *m* indicates the number of *CMS* samples. Furthermore, the *act* and *pred* superscripts are the actual and predicted values of the *CMS*.

It should be mentioned that the authors wrote several distinct codes in the Matlab environment and used each of them for a specific purpose: for (1) conducting the relevancy test, (2) constructing and testing the CNN model, (3) performing statistical analysis, and (4) creating graphs.

3. Results and Discussion

This section explains the process followed to determine the best topology of the CNN and evaluate its prediction accuracy.

3.1. Tuning the CNN Topology

Although it is possible to create the cascade neural network with arbitrary numbers of neuron layers, this study estimates the CO_2/CH_4 selectivity of MMMs using a single hidden layer CNN. All the designed CNNs include an input layer, one hidden layer, and an output layer. Independent variables constitute the input layer and, therefore, it is fixed. In addition, the number of output neurons is dictated by the number of dependent variables (i.e., one). Therefore, it is only necessary to determine the best number of hidden neurons to fine-tune the CNN topology.

The numbers of the hidden neurons of CNNs are changed from one to twelve during a trial-and-error process. In addition, ten models are developed per each number of hidden neurons. In summary, this study develops 120 CNNs and compares their accuracy to find the highest accurate one. Figure 2 reports the results of the ranking analysis performed on the 120 developed CNNs. It can be seen that the eighth developed CNN model with eleven hidden neurons has the best performance and achieves the first-rank position. Therefore, the CNN model with eleven hidden neurons, a tangent sigmoid in the hidden layer, and a logarithm sigmoid in the output layer is selected as the final model to estimate the CO_2/CH_4 selectivity of MMMs.

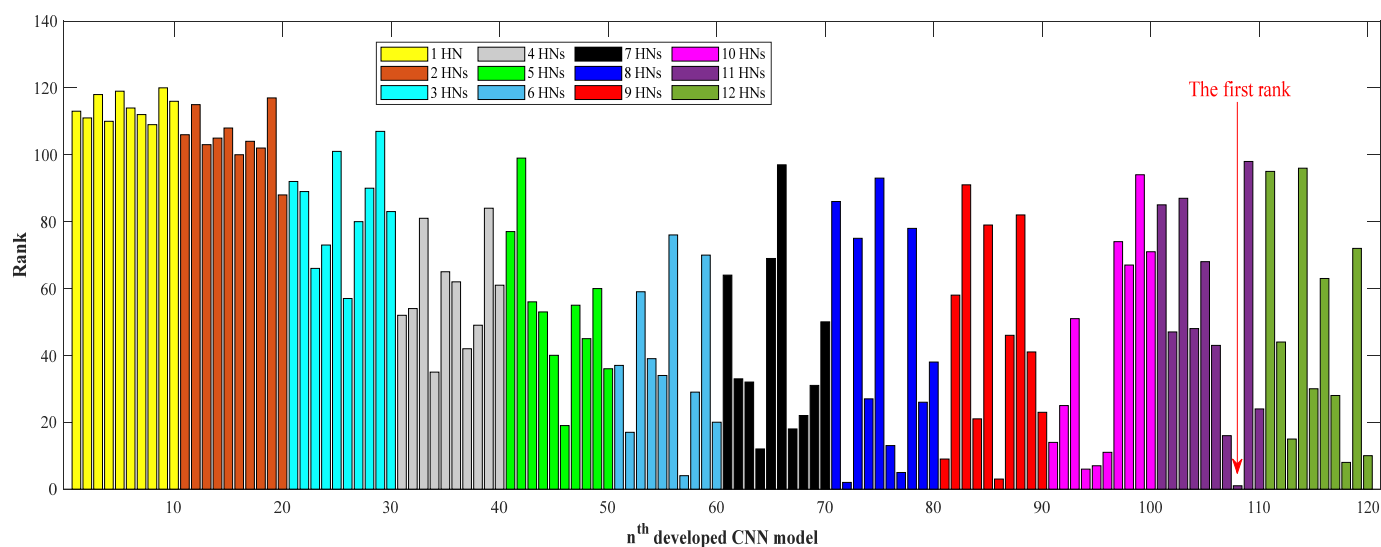


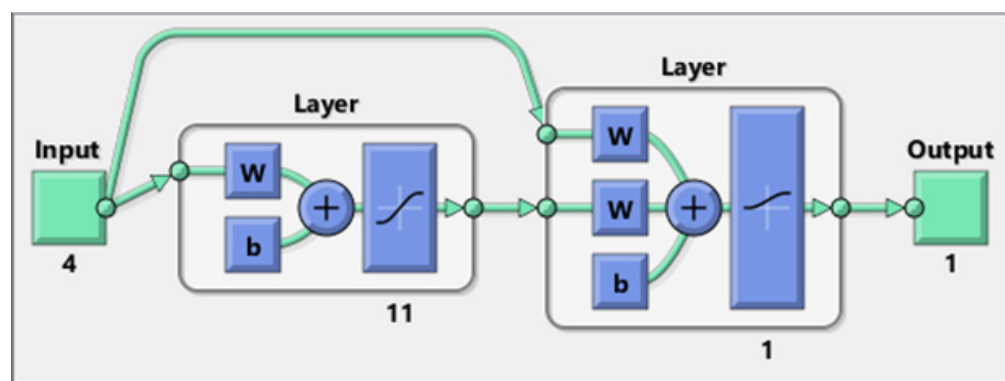
Figure 2. The procedure of the CNN topology tuning.

Table 2 introduces the numerical values of the AARD%, MSE, and R indices related to the CNN performance to estimate 118 CO_2/CH_4 selectivity samples of polymer/SAPO-34 membranes. The training, testing, and all datasets have been estimated with excellent AARDs of 2.31%, 6.36%, and 2.93%, respectively. The structure-tuned CNN has also predicted these three datasets with the MSE of 0.51, 7.32, and 1.55, respectively. The closeness of the observed R values to the one in the training and testing steps, and their combination, is another indication of the outstanding ability of the proposed CNN for simulating the considered separation task.

Table 2. Information on the obtained AARD%, MSE, and R by the best CNN model.

Dataset	AARD%	MSE	R
Training step	2.31	0.51	0.9988
Testing step	6.36	7.32	0.9860
All the data	2.93	1.55	0.9964

The key information related to the designed CNN has been presented in Figure 3. The feedforward connection between input/hidden and hidden/output layers, as well as the cascade connection between input/output layers, are observable in this figure. Moreover, four inputs are SAPO-34 dosage, polymer type, pressure, and temperature, while the CO₂/CH₄ selectivity of MMMs is the only output. This figure also shows two neuronal layers (i.e., hidden and output) with 11 and 1 neurons, respectively. The tangent and logarithm sigmoid transfer functions can be easily seen in the hidden and output layers.

**Figure 3.** Schematic of the designed CNN for estimating the CO₂/CH₄ selectivity of MMMs [65].

3.2. CNN Performance Evaluation

The cross-plot showing the predicted CO₂/CH₄ selectivity by the CNN versus actual values for the training, testing, and all datasets are depicted in Figure 4. This figure proves that the designed CNN has successfully mapped the estimated selectivity samples on their corresponding actual data in both training and testing steps. The R values related to the estimation of the training and testing groups are 0.9988 and 0.9860, respectively. These values state that the major parts of the predicted–actual symbols are located around the diagonal lines.

The relative deviation percent (i.e., Equation (8)) associated with estimating each experimental measurement of the actual CO₂/CH₄ selectivity of MMMs is shown in Figure 5. This figure shows that only four training and six testing CO₂/CH₄ selectivity samples have been estimated with an RD% higher than 5% or lower than −5%. It can be claimed that the proposed CNN model estimates 110 out of 118 actual CO₂/CH₄ selectivity samples with an excellent RD% in the range of −5% to 5%.

The residual error between experimental and calculated CO₂/CH₄ selectivity samples (i.e., Equation (9)) for the training and testing phases, as well as all the datasets, has been illustrated in Figure 6. This figure shows that the CNN estimates almost all the experimental selectivity samples with the RE ranges from −3 to +3. Few CO₂/CH₄ selectivity samples are estimated with a RE outside this narrow range.

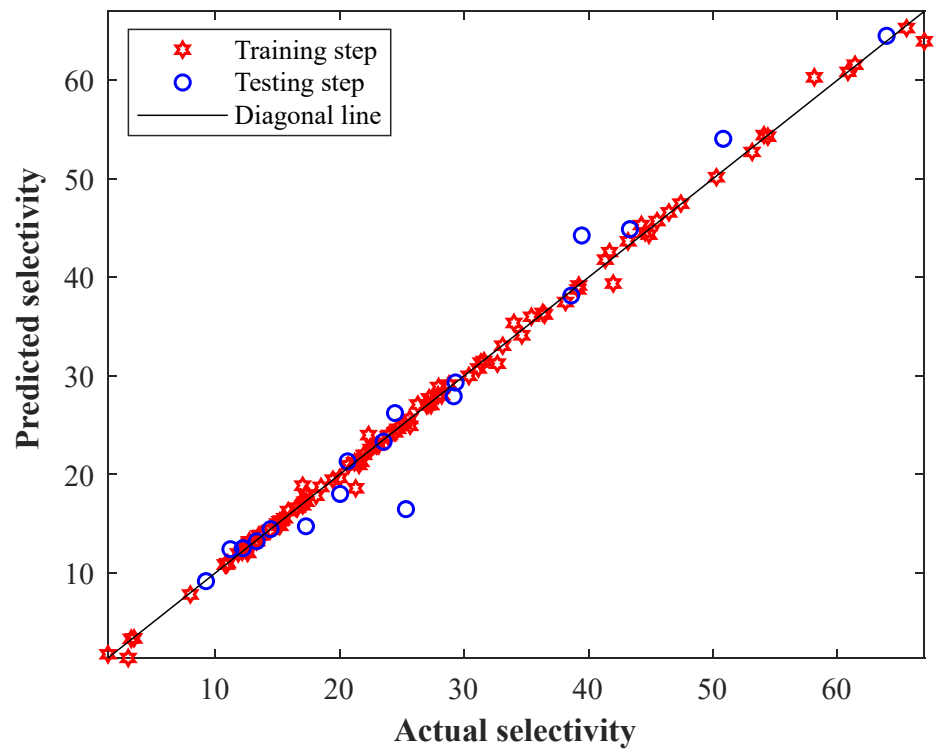


Figure 4. Cross-plot of the CNN predictions versus the actual CO₂/CH₄ selectivity of MMMs.

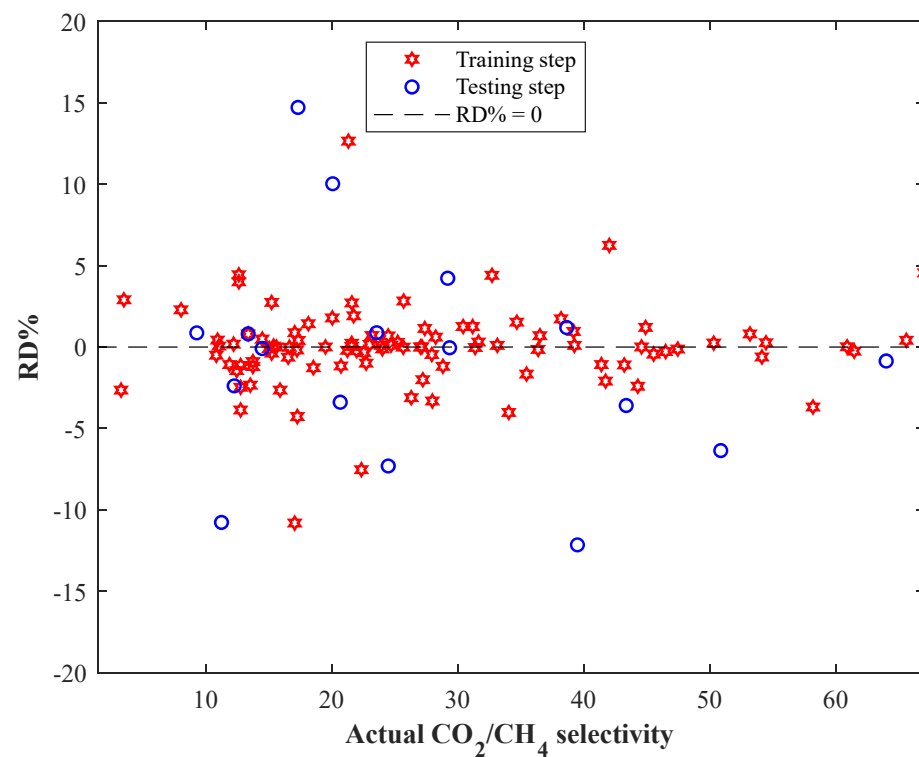


Figure 5. The observed RD% for estimating the CO₂/CH₄ selectivity of MMMs.

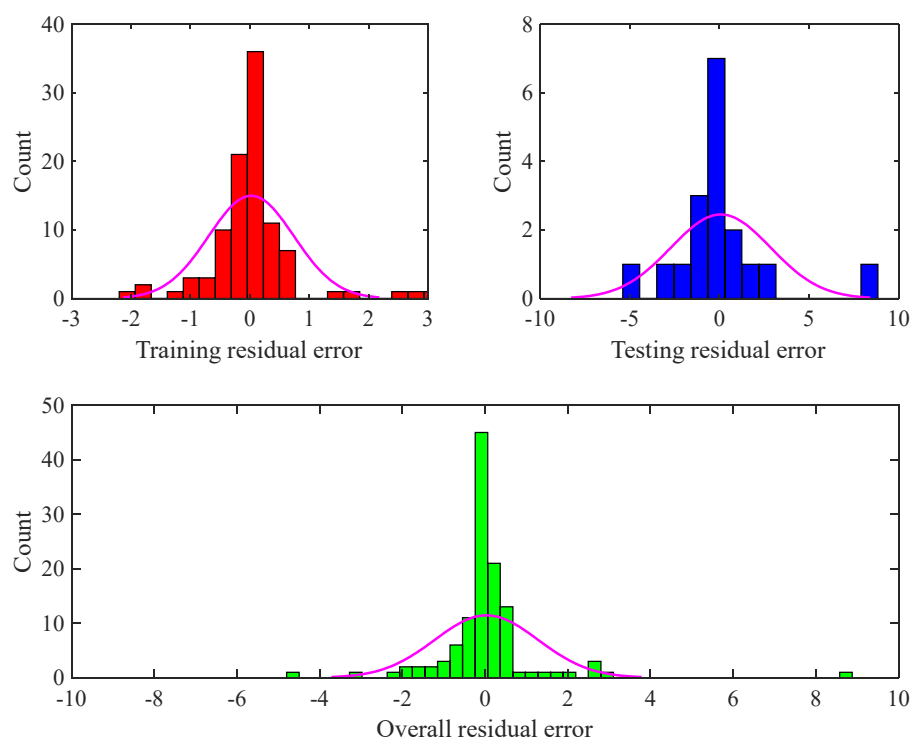


Figure 6. The observed residual error for estimating the training, testing, and overall databank.

3.3. Validation by Experimental Measurements

Figure 7 shows the experimental and CNN predictions for the training and testing sample of the CO_2/CH_4 selectivity of MMMs. Although the experimental CO_2/CH_4 selectivity measurements cover a relatively broad range (1.38–66.99) in different compositions of MMMs and operating conditions, the proposed CNN is able to precisely simulate the considered process. This figure also explains that 100 CO_2/CH_4 selectivity samples have been used in the training step and the remaining 18 samples are used in the testing step. It was previously reported that the proposed CNN estimates the training and testing datasets with excellent AARDs of 2.31% and 6.36%, respectively.

3.4. Investigating the Effect of Involved Features on the Selectivity

Figure 8 introduces experimental records and CNN predictions for the CO_2/CH_4 selectivity of polyurethane membrane and polyurethane-SAPO-34 MMM versus pressure at 298 K. This figure justifies the acceptable agreement between actual and predicted selectivity samples. This figure also shows that the CO_2/CH_4 selectivity of both membranes increases with increasing pressure and filler dose. Although Pearson's method correctly anticipated the filler effect on the selectivity, it provided a wrong result for the selectivity–pressure relationship. As mentioned before, this wrong prediction of the relevancy test is often related to the high level of scattering in the experimental data.

It is better to note that the relevancy test also anticipated a weak relationship between selectivity and pressure, but this analysis approves that the pressure is able to change selectivity sharply.

The pressure effect on the CO_2/CH_4 selectivity of Pebax 1074-based MMMs containing 20% SAPO-34 at two temperature levels (298 and 308 K) is depicted in Figure 9. The increasing effect of pressure and decreasing effect of temperature on the CO_2/CH_4 selectivity can be concluded from this figure. The relevancy test also confirmed an indirect relationship between selectivity and temperature.

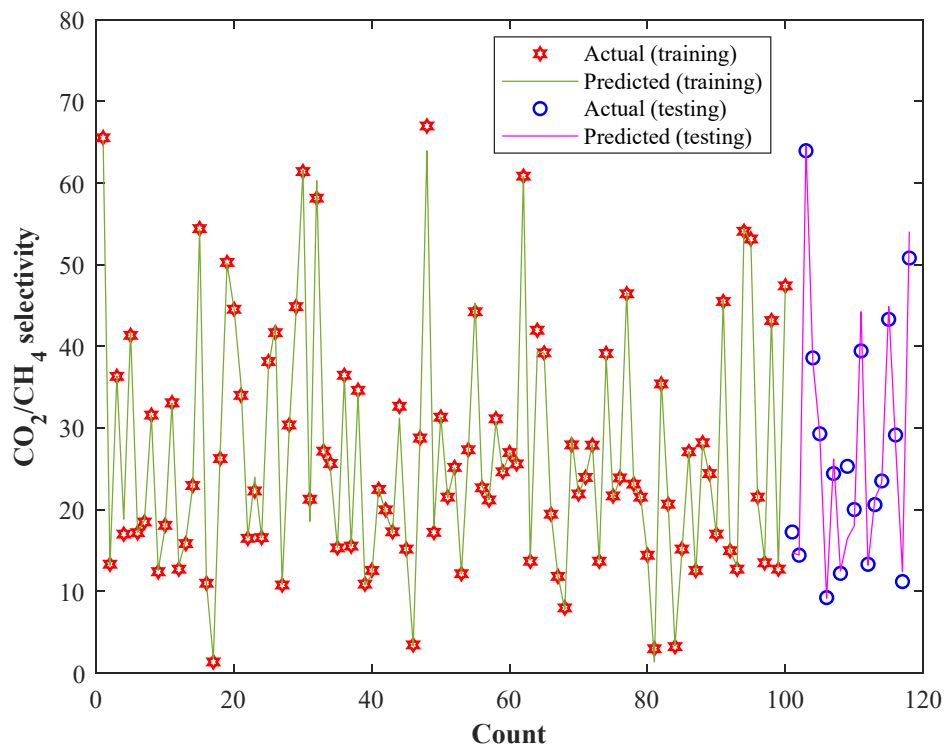


Figure 7. Actual CO₂/CH₄ selectivity of MMMs and their counterpart CNN estimations in the training as well as testing steps.

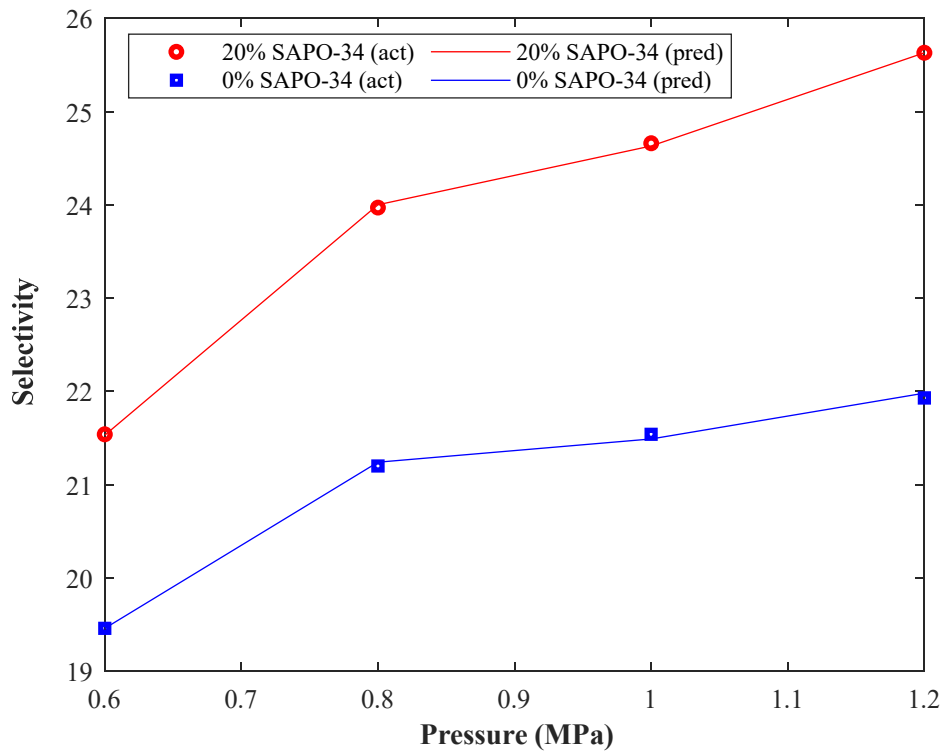


Figure 8. The dependency of CO₂/CH₄ selectivity of polyurethane-based MMMs on the pressure and filler dose (298 K).

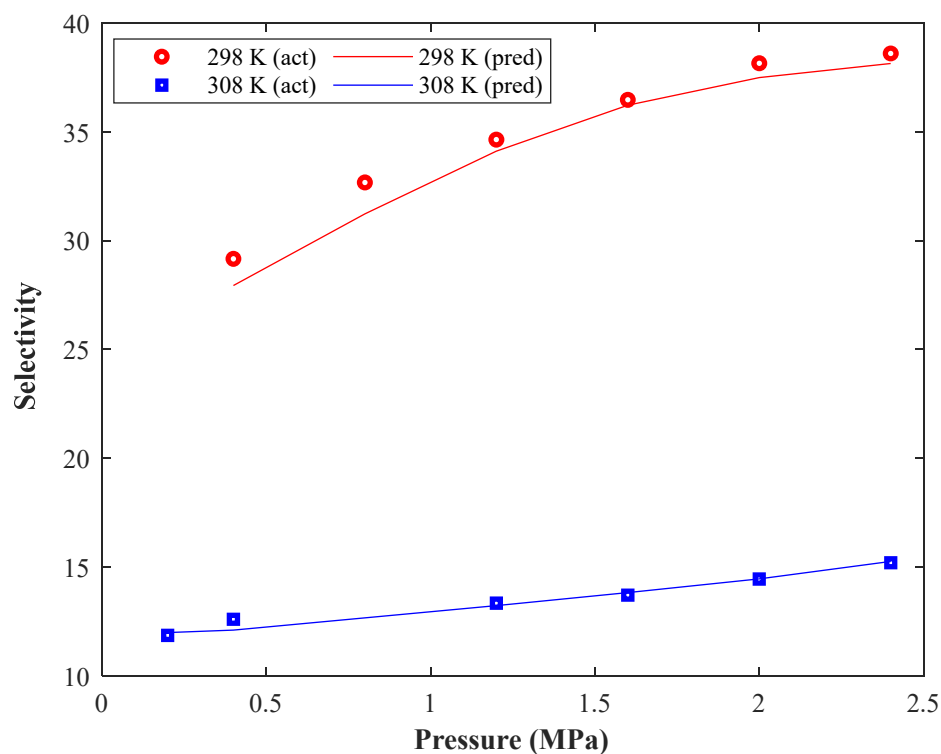


Figure 9. The dependency of CO_2/CH_4 selectivity of Pebax 1074-based MMMs on the pressure and temperature (20% SAPO-34).

It is better to note that Pearson's method also claimed that a weak relationship exists between selectivity and temperature, but this analysis approves that the temperature impact on the selectivity is strong.

4. Conclusions

This study aimed to estimate the CO_2/CH_4 selectivity of those mixed matrix membranes composed of polymeric substrates and with SAPO-34 zeolite as the filler. The cascade neural network was chosen to extract the relationship between the CO_2/CH_4 selectivity of the considered MMMs and the involved independent variables (i.e., filler dosage in polymeric matrices, polymer type, temperature, and pressure). Pearson's method proved that an acceptable degree of relevancy existed between the selectivity and the influential variables. This method identified that the SAPO-34 dosage in the composite membrane has the strongest direct effect on the CO_2/CH_4 selectivity of the considered MMMs. The CNN topology has been fine-tuned using trial-and-error and statistical analyses. The CNN with 11 hidden nodes estimate 118 actual selectivity samples with the AARD = 2.92%, MSE = 1.55, and R = 0.9964, is identified as the most accurate model for the considered task. Moreover, several graphical analyses, including cross-plot, residual error, relative deviation percent, and predicted versus actual graphs have further justified the outstanding performance of the proposed CNN for estimating the CO_2/CH_4 selectivity of the MMMs. Such a reliable model helps monitor the effect of MMM composition (polymer type and filler dosage) and operating conditions (pressure and temperature) on the potential CO_2/CH_4 selectivity.

Author Contributions: S.A.A.: writing—original draft, writing—review and editing, investigation, formal analysis, data curation, software; A.A.: writing—original draft, writing—review and editing, project administration, validation; A.P.: writing—original draft, writing—review and editing, methodology, resources; A.H.A.: writing—original draft, writing—review and editing, methodology, software; F.A.: resources, supervision; B.A.: writing—review and editing. All authors have read and agreed to the published version of the manuscript.

Funding: This research received no external funding.

Institutional Review Board Statement: Not applicable.

Informed Consent Statement: Not applicable.

Data Availability Statement: The study data analyzed in this article can be obtained by request from the corresponding author.

Acknowledgments: We acknowledge the support of the Deutsche Forschungsgemeinschaft (DFG—German Research Foundation) and the Open Access Publishing Fund of the Technical University of Darmstadt.

Conflicts of Interest: The authors declare no conflict of interest.

References

1. Pörtner, H.-O.; Roberts, D.C.; Adams, H.; Adler, C.; Aldunce, P.; Ali, E.; Begum, R.A.; Betts, R.; Kerr, R.B.; Biesbroek, R. *Climate Change 2022: Impacts, Adaptation and Vulnerability*; IPCC Sixth Assessment Report; Cambridge University Press: Cambridge, UK; New York, NY, USA, 2022.
2. Guo, B.; Wang, Y.; Zhou, H.; Hu, F. Can environmental tax reform promote carbon abatement of resource-based cities? Evidence from a quasi-natural experiment in China. *Environ. Sci. Pollut. Res.* **2022**, 1–13. [[CrossRef](#)] [[PubMed](#)]
3. Osman, A.I.; Chen, L.; Yang, M.; Msigwa, G.; Farghali, M.; Fawzy, S.; Rooney, D.W.; Yap, P.-S. Cost, environmental impact, and resilience of renewable energy under a changing climate: A review. *Environ. Chem. Lett.* **2023**, *21*, 741–764. [[CrossRef](#)]
4. Scarlat, N.; Dallemand, J.-F.; Fahl, F. Biogas: Developments and perspectives in Europe. *Renew. Energy* **2018**, *129*, 457–472. [[CrossRef](#)]
5. Zhao, C.; Xi, M.; Huo, J.; He, C.; Fu, L. Computational design of BC₃N₂ based single atom catalyst for dramatic activation of inert CO₂ and CH₄ gasses into CH₃COOH with ultralow CH₄ dissociation barrier. *Chin. Chem. Lett.* **2023**, *34*, 107213. [[CrossRef](#)]
6. Qu, M.; Chen, Z.; Sun, Z.; Zhou, D.; Xu, W.; Tang, H.; Gu, H.; Liang, T.; Hu, P.; Li, G. Rational design of asymmetric atomic Ni-P₁N₃ active sites for promoting electrochemical CO₂ reduction. *Nano Res.* **2023**, *16*, 2170–2176. [[CrossRef](#)]
7. He, S.; Zhu, B.; Li, S.; Zhang, Y.; Jiang, X.; Lau, C.H.; Shao, L. Recent progress in PIM-1 based membranes for sustainable CO₂ separations: Polymer structure manipulation and mixed matrix membrane design. *Sep. Purif. Technol.* **2022**, *284*, 120277. [[CrossRef](#)]
8. Xu, G.; Li, L.; Yang, Y.; Tian, L.; Liu, T.; Zhang, K. A novel CO₂ cryogenic liquefaction and separation system. *Energy* **2012**, *42*, 522–529. [[CrossRef](#)]
9. Liu, R.; Shi, X.; Wang, C.; Gao, Y.; Xu, S.; Hao, G.; Chen, S.; Lu, A. Advances in post-combustion CO₂ capture by physical adsorption: From materials innovation to separation practice. *ChemSusChem* **2021**, *14*, 1428–1471. [[CrossRef](#)]
10. Aghel, B.; Janati, S.; Wongwises, S.; Shadloo, M.S. Review on CO₂ capture by blended amine solutions. *Int. J. Greenh. Gas Control* **2022**, *119*, 103715. [[CrossRef](#)]
11. Waldman, R.Z.; Gao, F.; Phillip, W.A.; Darling, S.B. Maximizing selectivity: An analysis of isoporous membranes. *J. Membr. Sci.* **2021**, *633*, 119389. [[CrossRef](#)]
12. Karimi, M.; Rodrigues, A.E.; Silva, J.A.C. Designing a simple volumetric apparatus for measuring gas adsorption equilibria and kinetics of sorption. Application and validation for CO₂, CH₄ and N₂ adsorption in binder-free beads of 4A zeolite. *Chem. Eng. J.* **2021**, *425*, 130538. [[CrossRef](#)]
13. Karimi, M.; Diaz de Tuesta, J.L.; Carmem, C.N.; Gomes, H.T.; Rodrigues, A.E.; Silva, J.A.C. Compost from Municipal Solid Wastes as a Source of Biochar for CO₂ Capture. *Chem. Eng. Technol.* **2020**, *43*, 1336–1349. [[CrossRef](#)]
14. Vinoba, M.; Bhagiyalakshmi, M.; Alqaheem, Y.; Alomair, A.A.; Pérez, A.; Rana, M.S. Recent progress of fillers in mixed matrix membranes for CO₂ separation: A review. *Sep. Purif. Technol.* **2017**, *188*, 431–450. [[CrossRef](#)]
15. Zunita, M.; Natola, W.; David, M.; Lugito, G. Integrated Metal Organic Framework/Ionic Liquid-Based Composite Membrane for CO₂ Separation. *Chem. Eng. J. Adv.* **2022**, *11*, 100320. [[CrossRef](#)]
16. Basu, S.; Khan, A.L.; Cano-Odena, A.; Liu, C.; Vankelecom, I.F.J. Membrane-based technologies for biogas separations. *Chem. Soc. Rev.* **2010**, *39*, 750–768. [[CrossRef](#)] [[PubMed](#)]
17. Lubi, M.C.; Thachil, E.T. Cashew nut shell liquid (CNSL)-a versatile monomer for polymer synthesis. *Des. Monomers Polym.* **2000**, *3*, 123–153. [[CrossRef](#)]
18. Chung, T.; Shao, L.; Tin, P.S. Surface modification of polyimide membranes by diamines for H₂ and CO₂ separation. *Macromol. Rapid Commun.* **2006**, *27*, 998–1003. [[CrossRef](#)]
19. Haider, B.; Dilshad, M.R.; Rehman, M.A.U.; Schmitz, J.V.; Kaspereit, M. Highly permeable novel PDMS coated asymmetric polyethersulfone membranes loaded with SAPO-34 zeolite for carbon dioxide separation. *Sep. Purif. Technol.* **2020**, *248*, 116899. [[CrossRef](#)]
20. Wu, R.; Tan, Y.; Meng, F.; Zhang, Y.; Huang, Y.-X. PVDF/MAF-4 composite membrane for high flux and scaling-resistant membrane distillation. *Desalination* **2022**, *540*, 116013. [[CrossRef](#)]

21. Huang, G.; Isfahani, A.P.; Muchtar, A.; Sakurai, K.; Shrestha, B.B.; Qin, D.; Yamaguchi, D.; Sivaniah, E.; Ghalei, B. Pebax/ionic liquid modified graphene oxide mixed matrix membranes for enhanced CO₂ capture. *J. Membr. Sci.* **2018**, *565*, 370–379. [[CrossRef](#)]
22. Kosinov, N.; Gascon, J.; Kapteijn, F.; Hensen, E.J.M. Recent developments in zeolite membranes for gas separation. *J. Membr. Sci.* **2016**, *499*, 65–79. [[CrossRef](#)]
23. Melgar, V.M.A.; Kim, J.; Othman, M.R. Zeolitic imidazolate framework membranes for gas separation: A review of synthesis methods and gas separation performance. *J. Ind. Eng. Chem.* **2015**, *28*, 1–15. [[CrossRef](#)]
24. Usman, M.; Ghanem, A.S.; Niaz Ali Shah, S.; Garba, M.D.; Yusuf Khan, M.; Khan, S.; Humayun, M.; Laeeq Khan, A. A Review on SAPO-34 Zeolite Materials for CO₂ Capture and Conversion. *Chem. Rec.* **2022**, *22*, e202200039. [[CrossRef](#)] [[PubMed](#)]
25. Li, S.; Falconer, J.L.; Noble, R.D. SAPO-34 membranes for CO₂/CH₄ separation. *J. Membr. Sci.* **2004**, *241*, 121–135. [[CrossRef](#)]
26. Rimaz, S.; Kosari, M.; Zarinejad, M.; Ramakrishna, S. A comprehensive review on sustainability-motivated applications of SAPO-34 molecular sieve. *J. Mater. Sci.* **2022**, *57*, 848–886. [[CrossRef](#)]
27. Zhang, H.; Zou, Q.; Ju, Y.; Song, C.; Chen, D. Distance-based Support Vector Machine to Predict DNA N⁶-methyladenine Modification. *Curr. Bioinform.* **2022**, *17*, 473–482.
28. Si, Z.; Yang, M.; Yu, Y.; Ding, T. Photovoltaic power forecast based on satellite images considering effects of solar position. *Appl. Energy* **2021**, *302*, 117514. [[CrossRef](#)]
29. Sun, P.; Ma, H.; Li, S.; Yao, H.; Zhang, R. Prediction of second-order rate constants between carbonate radical and organics by deep neural network combined with molecular fingerprints. *Chin. Chem. Lett.* **2022**, *33*, 438–441. [[CrossRef](#)]
30. Samanta, A.; Chowdhuri, S.; Williamson, S.S. Machine learning-based data-driven fault detection/diagnosis of lithium-ion battery: A critical review. *Electronics* **2021**, *10*, 1309. [[CrossRef](#)]
31. Wieland, M.; Pittore, M. Performance evaluation of machine learning algorithms for urban pattern recognition from multi-spectral satellite images. *Remote Sens.* **2014**, *6*, 2912–2939. [[CrossRef](#)]
32. Jiménez-Carvelo, A.M.; González-Casado, A.; Bagur-González, M.G.; Cuadros-Rodríguez, L. Alternative data mining/machine learning methods for the analytical evaluation of food quality and authenticity—A review. *Food Res. Int.* **2019**, *122*, 25–39. [[CrossRef](#)] [[PubMed](#)]
33. Wang, Y.; Seo, B.; Wang, B.; Zamel, N.; Jiao, K.; Adroher, X.C. Fundamentals, materials, and machine learning of polymer electrolyte membrane fuel cell technology. *Energy AI* **2020**, *1*, 100014. [[CrossRef](#)]
34. Nandi, B.K.; Moparthi, A.; Uppaluri, R.; Purkait, M.K. Treatment of oily wastewater using low cost ceramic membrane: Comparative assessment of pore blocking and artificial neural network models. *Chem. Eng. Res. Des.* **2010**, *88*, 881–892. [[CrossRef](#)]
35. Waqas, S.; Harun, N.Y.; Sambudi, N.S.; Arshad, U.; Nordin, N.A.H.M.; Bilad, M.R.; Saeed, A.A.H.; Malik, A.A. SVM and ANN Modelling Approach for the Optimization of Membrane Permeability of a Membrane Rotating Biological Contactor for Wastewater Treatment. *Membranes* **2022**, *12*, 821. [[CrossRef](#)]
36. Rezakazemi, M.; Dashti, A.; Asghari, M.; Shirazian, S. H₂-selective mixed matrix membranes modeling using ANFIS, PSO-ANFIS, GA-ANFIS. *Int. J. Hydrog. Energy* **2017**, *42*, 15211–15225. [[CrossRef](#)]
37. Chamani, H.; Yazgan-Birgi, P.; Matsuura, T.; Rana, D.; Ali, M.I.H.; Arafat, H.A.; Lan, C.Q. CFD-based genetic programming model for liquid entry pressure estimation of hydrophobic membranes. *Desalination* **2020**, *476*, 114231. [[CrossRef](#)]
38. Chen, Y.; Yu, G.; Long, Y.; Teng, J.; You, X.; Liao, B.Q.; Lin, H. Application of radial basis function artificial neural network to quantify interfacial energies related to membrane fouling in a membrane bioreactor. *Bioresour. Technol.* **2019**, *293*, 122103. [[CrossRef](#)]
39. Tyagi, A.; Iqbal, J.; Meena, Y.K.; Jain, M. Modeling and optimization of neodymium ion separation by liquid membrane using Artificial Neural Network coupled with Genetic Algorithm. *Chem. Eng. Res. Des.* **2022**, *187*, 151–163. [[CrossRef](#)]
40. Gasós, A.; Becattini, V.; Brunetti, A.; Barbieri, G.; Mazzotti, M. Process performance maps for membrane-based CO₂ separation using artificial neural networks. *Int. J. Greenh. Gas Control* **2023**, *122*, 103812. [[CrossRef](#)]
41. Peydayesh, M.; Asarehpour, S.; Mohammadi, T.; Bakhtiari, O. Preparation and characterization of SAPO-34–Matrimid[®] 5218 mixed matrix membranes for CO₂/CH₄ separation. *Chem. Eng. Res. Des.* **2013**, *91*, 1335–1342. [[CrossRef](#)]
42. Zhao, D.; Ren, J.; Li, H.; Hua, K.; Deng, M. Poly (amide-6-b-ethylene oxide)/SAPO-34 mixed matrix membrane for CO₂ separation. *J. Energy Chem.* **2014**, *23*, 227–234. [[CrossRef](#)]
43. Omrani, H.; Naser, I.; Rafie Zadeh, M. Experimental and numerical study of CO₂/CH₄ separation using sa-po-34/pes hollow fiber membrane. *Iran. J. Chem. Chem. Eng.* **2020**, *40*, 841–852.
44. Kiamehr, Y.; Naser, I.; Rafizadeh, M.; Mohammadi, A.H. Preparation and Characterization of Amine-functional SAPO-34 Mixed Matrix Membranes for CO₂/CH₄ Separation. *Iran. J. Energy Environ.* **2022**, *13*, 238–247. [[CrossRef](#)]
45. Mohshim, D.F.; Mukhtar, H.; Man, Z. The effect of incorporating ionic liquid into polyethersulfone-SAPO34 based mixed matrix membrane on CO₂ gas separation performance. *Sep. Purif. Technol.* **2014**, *135*, 252–258. [[CrossRef](#)]
46. Sodeifian, G.; Raji, M.; Asghari, M.; Rezakazemi, M.; Dashti, A. Polyurethane-SAPO-34 mixed matrix membrane for CO₂/CH₄ and CO₂/N₂ separation. *Chin. J. Chem. Eng.* **2019**, *27*, 322–334. [[CrossRef](#)]
47. Junaidi, M.U.M.; Leo, C.P.; Ahmad, A.L.; Kamal, S.N.M.; Chew, T.L. Carbon dioxide separation using asymmetric polysulfone mixed matrix membranes incorporated with SAPO-34 zeolite. *Fuel Process. Technol.* **2014**, *118*, 125–132. [[CrossRef](#)]
48. Rabiee, H.; Alsadat, S.M.; Soltanieh, M.; Mousavi, S.A.; Ghadimi, A. Gas permeation and sorption properties of poly (amide-12-b-ethyleneoxide)(Pebax1074)/SAPO-34 mixed matrix membrane for CO₂/CH₄ and CO₂/N₂ separation. *J. Ind. Eng. Chem.* **2015**, *27*, 223–239. [[CrossRef](#)]

49. Junaidi, M.U.M.; Khoo, C.P.; Leo, C.P.; Ahmad, A.L. The effects of solvents on the modification of SAPO-34 zeolite using 3-aminopropyl trimethoxy silane for the preparation of asymmetric polysulfone mixed matrix membrane in the application of CO₂ separation. *Microporous Mesoporous Mater.* **2014**, *192*, 52–59. [[CrossRef](#)]
50. Junaidi, M.U.M.; Leo, C.P.; Ahmad, A.L.; Ahmad, N.A. Fluorocarbon functionalized SAPO-34 zeolite incorporated in asymmetric mixed matrix membranes for carbon dioxide separation in wet gases. *Microporous Mesoporous Mater.* **2015**, *206*, 23–33. [[CrossRef](#)]
51. Ahmad, N.N.R.; Leo, C.P.; Mohammad, A.W.; Ahmad, A.L. Modification of gas selective SAPO zeolites using imidazolium ionic liquid to develop polysulfone mixed matrix membrane for CO₂ gas separation. *Microporous Mesoporous Mater.* **2017**, *244*, 21–30. [[CrossRef](#)]
52. Messaoud, S.B.; Takagaki, A.; Sugawara, T.; Kikuchi, R.; Oyama, S.T. Mixed matrix membranes using SAPO-34/polyetherimide for carbon dioxide/methane separation. *Sep. Purif. Technol.* **2015**, *148*, 38–48. [[CrossRef](#)]
53. Hosseini, S.; Khandakar, A.; Chowdhury, M.E.H.; Ayari, M.A.; Rahman, T.; Chowdhury, M.H.; Vaferi, B. Novel and robust machine learning approach for estimating the fouling factor in heat exchangers. *Energy Rep.* **2022**, *8*, 8767–8776. [[CrossRef](#)]
54. Xie, J.; Liu, X.; Lao, X.; Vaferi, B. Hydrogen solubility in furfural and furfuryl bio-alcohol: Comparison between the reliability of intelligent and thermodynamic models. *Int. J. Hydrog. Energy* **2021**, *46*, 36056–36068. [[CrossRef](#)]
55. Hagan, M.T.; Demuth, H.B.; Beale, M. *Neural Network Design*; PWS Publishing Co.: Boston, MA, USA, 1997; ISBN 0534943322.
56. Guidotti, R.; Monreale, A.; Ruggieri, S.; Turini, F.; Giannotti, F.; Pedreschi, D. A survey of methods for explaining black box models. *ACM Comput. Surv.* **2018**, *51*, 1–42. [[CrossRef](#)]
57. Leperi, K.T.; Yancy-Caballero, D.; Snurr, R.Q.; You, F. 110th anniversary: Surrogate models based on artificial neural networks to simulate and optimize pressure swing adsorption cycles for CO₂ capture. *Ind. Eng. Chem. Res.* **2019**, *58*, 18241–18252. [[CrossRef](#)]
58. Gazzaz, N.M.; Yusoff, M.K.; Aris, A.Z.; Juahir, H.; Ramli, M.F. Artificial neural network modeling of the water quality index for Kinta River (Malaysia) using water quality variables as predictors. *Mar. Pollut. Bull.* **2012**, *64*, 2409–2420. [[CrossRef](#)] [[PubMed](#)]
59. Shi, X.; Fortune, K.; Smithlin, R.; Akin, M.; Fay, L. Exploring the performance and corrosivity of chloride deicer solutions: Laboratory investigation and quantitative modeling. *Cold Reg. Sci. Technol.* **2013**, *86*, 36–44. [[CrossRef](#)]
60. Capizzi, G.; Sciuto, G.L.; Monforte, P.; Napoli, C. Cascade Feed Forward Neural Network-based Model for Air Pollutants Evaluation of Single Monitoring Stations in Urban Areas. *Int. J. Electron. Telecommun.* **2015**, *61*, 327–332. [[CrossRef](#)]
61. Shaban, K.; El-Hag, A.; Matveev, A. A cascade of artificial neural networks to predict transformers oil parameters. *IEEE Trans. Dielectr. Electr. Insul.* **2009**, *16*, 516–523. [[CrossRef](#)]
62. Calisir, T.; Çolak, A.B.; Aydin, D.; Dalkilic, A.S.; Baskaya, S. Artificial neural network approach for investigating the impact of convector design parameters on the heat transfer and total weight of panel radiators. *Int. J. Therm. Sci.* **2023**, *183*, 107845. [[CrossRef](#)]
63. Karimi, M.; Hosin Alibak, A.; Seyed Alizadeh, S.M.; Sharif, M.; Vaferi, B. Intelligent modeling for considering the effect of bio-source type and appearance shape on the biomass heat capacity. *Meas. J. Int. Meas. Confed.* **2022**, *189*, 110529. [[CrossRef](#)]
64. Alibak, A.H.; Alizadeh, S.M.; Davodi Monjezi, S.; Alizadeh, A.; Alobaid, F.; Aghel, B. Developing a Hybrid Neuro-Fuzzy Method to Predict Carbon Dioxide (CO₂) Permeability in Mixed Matrix Membranes Containing SAPO-34 Zeolite. *Membranes* **2022**, *12*, 1147. [[CrossRef](#)] [[PubMed](#)]
65. *MATLAB and Artificial Neural Networks Toolbox (Release 2019a)*; The MathWorks, Inc.: Natick, MA, USA, 2019.

Disclaimer/Publisher's Note: The statements, opinions and data contained in all publications are solely those of the individual author(s) and contributor(s) and not of MDPI and/or the editor(s). MDPI and/or the editor(s) disclaim responsibility for any injury to people or property resulting from any ideas, methods, instructions or products referred to in the content.